Heliyon 10 (2024) e40796

Contents lists available at ScienceDirect

Heliyon

journal homepage: www.cell.com/heliyon

Research article

The response to shock loads of Ni-MOF and NiO NPs on aerobic granular sludge and algal-bacterial aerobic granular sludge

Alfonz Kedves [a,*], Çağdaş Yavuz [a], Orsolya Kedves [b], Henrik Haspel [a,c], Zoltán Kónya [a,c]

[a] Department of Applied and Environmental Chemistry, University of Szeged, Szeged, Hungary
[b] Department of Microbiology, Faculty of Science and Informatics, University of Szeged, Szeged, Hungary
[c] HUN-REN Reaction Kinetics and Surface Chemistry Research Group, Szeged, Hungary

ARTICLE INFO

Keywords:
Aerobic granular sludge
Algal-bacterial aerobic granular sludge
Nickel oxide nanoparticles
Nickel metal-organic framework
Wastewater treatment

ABSTRACT

Currently, the increasing use of nickel metal-organic frameworks (Ni-MOF) and nickel oxide nanoparticles (NiO NPs) has raised concerns regarding their potential environmental impact on wastewater treatment systems. Herein, the responses of aerobic granular sludge (AGS) and algal-bacterial aerobic granular sludge (AB-AGS) to Ni-MOF and NiO NPs were investigated. The results showed that Ni-MOF concentrations of 50, 100, and 200 mg/L significantly reduced nutrient removal in both systems, particularly affecting ammonia, nitrite, and phosphorus removal, while denitrification processes remained stable. AB-AGS exhibited greater tolerance to nickel than AGS, likely due to its higher content of extracellular polymeric substances (EPSs), in which the algae were embedded, indicating a robust bacterial-algal symbiotic system. Conversely, NiO NPs had no adverse effects on bioreactor performance, likely due to their insolubility and integration into the sludge matrix. This research provides valuable insights into the potential future applications of AGS and AB-AGS technologies for treating wastewater contaminated with nickel and other heavy metals, highlighting the superior resilience of AB-AGS to nickel exposure.

1. Introduction

Nickel oxide nanoparticles (NiO NPs) have found widespread applications in optoelectronic and energy storage devices such as LEDs [1], solar cells, electrochromic coatings [2], and lithium-ion batteries [3], due to their diverse chemical properties. Moreover, their potential use in gas separation and storage [4,5], catalysts [6], microbial electrolysis cells [7], glucose sensors [8], Li-S batteries [8] and electrochemical energy storage fields [9] has garnered significant interest. Metal-organic frameworks (MOFs), composed of an inorganic metal node and organic ligands (primarily oxygen polydentate organic ligands, basic nitrogen, or aromatic acids), have emerged as promising materials for various applications [10,11]. With their two- or three-dimensional network-like crystal structures, MOFs offer large surface areas, high pore volumes, and adjustable frameworks, making them suitable for use as electrodes in supercapacitors [12,13]. Despite their growing use in commercial production, Ni-based materials have raised concerns due to their potential effects on human tissues, aquatic and terrestrial animals, bacteria, and various organisms [14,15]. Several studies have shown that Ni-based nanoparticles can induce cytotoxicity and stimulate inflammatory responses in human cells [16].

Nickel is an essential trace element; however, in higher concentrations, it can negatively affect microorganisms [17], plants [18],

* Corresponding author. Department of Applied and Environmental Chemistry, University of Szeged, H-6720 Szeged, Rerrich Béla tér 1, Hungary.
E-mail address: kedvesalfonz@chem.u-szeged.hu (A. Kedves).

https://doi.org/10.1016/j.heliyon.2024.e40796
Received 17 April 2024; Received in revised form 26 November 2024; Accepted 27 November 2024
Available online 29 November 2024

and human health [19]. Hence, the investigation of any potential negative effects is imperative. Raju et al. [20] reported that Ni-MOFs have an inhibitory effect on the formation of biofilms, with an LC_{50} around 140 μg/mL in the case of *Artemia salina*, while Li et al. [21] reported the toxic effects of metal-organic frameworks on *Chlamydomonas reinhardtii* model green algae. Furthermore, Ag/Ni-MOF and Cu/Ni-MOF complexes exhibited excellent antimicrobial activity against *Bacillus subtilis*, *Escherichia coli*, *Pseudomonas aeruginos*a, *Candida albicans*, and *Salmonella* spp [22,23]. Previous studies have reported that NiO NPs exert biotoxic effects on microorganisms, such as *Escherichia coli*, *Bacillus subtilis*, *Streptococcus aureus,* and *Artemia salina* [24,25]. The investigated nanoparticles also induced phytotoxicity in tomatoes [26] and *Abelmoschus esculentus* [27]. Xiao et al. [28] reported that NiO NPs (0.1 and 1 mg/L) reduced the nitrogen removal rate and microbial diversity in constructed wetlands, while Oukarroum et al. [29] observed a 75 % decrease in the chlorophyll content of green algal cells after the addition of NiO NPs at 0.1 mg/L. The emerging and promising Ni-MOF will be used more widely due to their periodic network structure, good thermal stability, and specific surface area. While NiO NPs are already extensively utilized, they are expected to be integrated into aquatic and wastewater treatment systems [30–32]. Wang et al. [33] investigated the effects of NiO NPs (0–60 mg/L) on activated sludge (AS), revealing that concentrations exceeding 5 mg/L had a detrimental impact on enzymatic activity and the removal of organic matter, phosphorus, and nitrogen, while the nickel concentration in the effluent water continuously increased. Xu et al. [16] reported that NiO NPs, when present at concentrations exceeding 10 mg/L, caused a significant decrease in nitrogen removal and microbial community richness in anammox biogranules. In anaerobic granules, the nanoparticles also reduced enzyme activity, leading to a gradual decrease in methane yield [34].

The most commonly used technology in wastewater treatment is the conventional activated sludge (CAS) process [35]. The microorganisms employed in this process are highly sensitive to various pollutants in wastewater [36], which necessitates the development of new technologies. Aerobic granular sludge (AGS) and algal-bacterial aerobic granular sludge (AB-AGS) technologies represent novel and emerging biological processes for wastewater treatment [37,38]. Both AGS and AB-AGS achieve the simultaneous removal of carbon, nitrogen, phosphorus, and other pollutants within a single sludge system [39]. Granulated sludge exhibits distinct advantages compared to AS, featuring a dense and compact structure, excellent performance in organic and ammonia removal, excellent sludge settleability, a high potential for nutrient recovery, and enhanced resilience to toxicants [40]. Aerobic granules can be formed from activated sludge using the biomass washout method, while algal-bacterial granulated sludge can be obtained either from activated sludge or granulated sludge under light irradiation in a photo-sequencing batch reactor (PSBR) [41,42]. Extracellular polymeric substances (EPSs) play a vital role in granulation, facilitating faster attachment of microorganisms to each other. Furthermore, microorganisms and algae are embedded in the polymer matrix, providing a shield against harmful substances [37,38]. These innovative technologies have already demonstrated their capability of treat landfill leachate [41,43], pharmaceuticals [44,45], and textile dyes [46,47].

Earlier research examined the impact of various nanoparticles, including zinc oxide (ZnO NPs), cupric oxide (CuO NPs), silver (Ag NPs), silicon dioxide (SiO_2 NPs), and titanium dioxide (TiO_2 NPs) on AGS and AB-AGS wastewater treatment technologies. Quan et al. [48] observed a decrease in the microbial activity of nitrification and denitrification in AGS after the addition of Ag NPs at concentrations of 5 and 50 mg/L. Li et al. [49] reported that CuO NPs at 5 mg/L did not negatively affect nutrient removal in granular sludge. Contrary to these findings, Zheng et al. [50] reported a decrease in the nitrogen and phosphorus removal rates at a concentration of 5 mg/L, while the negative effect of nanoparticles increased as their concentrations rose to 50 mg/L. Jiang et al. [51] compared the potential negative effects of SiO_2 and TiO_2 NPs at 50 mg/L in AGS. They found that SiO_2 significantly reduced protein content and sludge settleability, while TiO_2 improved these properties. Additionally, nitrogen removal deteriorated after exposure to titanium nanoparticles. In another study, the authors investigated the effect of TiO_2 NPs on AB-AGS and did not find any negative effects on the properties of sludge or on the removal efficiency [52]. When the effect of ZnO NPs on AB-AGS in a PSBR was investigated, the authors observed a slight decrease in bioreactor performance, likely attributed to a symbiotic relationship between the algae and bacterial cells [53]. To date, no previous study has investigated the effects of a Ni-MOF and NiO NPs on bacterial and algal-bacterial granular sludge wastewater treatment processes.

The emerging use of nickel-based materials, particularly Ni-MOF and NiO NPs, in various industries has raised concerns about their potential environmental impact on wastewater treatment processes. Despite their growing application, limited research has been conducted to assess the effects of these materials on advanced wastewater treatment systems such as AGS and AB-AGS. The main purpose of this study is to evaluate the short-term effects of Ni-MOF and NiO NPs at varying concentrations (1–200 mg/L) on the performance of AGS SBR and AB-AGS PSBR systems, specifically focusing on nutrient removal, microbial activity, EPS production, and sludge properties. The goal is to provide fundamental knowledge on the impact of Ni-MOF and NiO NPs on these distinct bacterial and algal-bacterial aggregates within granulated sludge. This research is important because understanding the tolerance and resilience of AGS and AB-AGS to these nanoparticles will provide valuable insights into their potential application in treating wastewater contaminated with metal nanoparticles.

2. Material and methods

2.1. Preparation and characterization of Ni-MOF and NiO NPs

For the synthesis of Ni-MOF and NiO nanoparticles, nickel nitrate hexahydrate ($Ni(NO_3)_2{\cdot}6H_2O$, 99 %), 2-methylimidazole ($C_4H_6N_2$, 99 %), methanol and ethylene glycol were used. Chemicals were purchased from Sigma-Aldrich and used without further purifications. To synthesize Ni-MOF with the crystal structure of ZIF-8, 15 mmol 2-methylimidazole (2-mIM) was dissolved in 30 mL of methanol and mixed with a solution of 4 mmol nickel(II) nitrate hexahydrate dissolved in 20 mL methanol, then stirred magnetically at room temperature for 1 h. The resulting sediment was subsequently extracted via centrifugation (5000 rpm, 5 min), and washed three

times with deionized (DI) water and ethanol. The product was dried overnight at 60 °C in a drying oven, yielding a light green Ni-MOF powder [54]. The NiO NPs were prepared according to Zeng et al. [55] with minor modifications. In the solvothermal synthesis of NiO NPs, 1.18 mmol of Ni-salt was dissolved in 45 mL ethylene glycol and stirred at 40 °C for 1 h. The solution was then transferred to a 50 mL PTFE-lined stainless-steel autoclave and kept at 175 °C for 10 h. The resulting suspension was centrifuged and washed, and dried at 50 °C. The collected powder was annealed at 450 °C for 2 h in a muffle furnace to obtain the NiO NPs. Fig. 1 displays a schematic representation of the samples.

X-ray diffraction (XRD) patterns were recorded using a Rigaku Miniflex-II X-ray diffractometer (Cu Kα radiation, $\lambda = 1.54$ Å) operated at 30 kV and 30 mA with a scanning rate of 5° min^{-1} over a 2θ range of 5°–80°. Raman spectra were measured using a Bruker Senterra II Raman microscope using a 532 nm laser excitation at 12.5 mW power. Fourier-transform infrared spectroscopy (FT-IR) was carried out using a Bruker Vertex 70 instrument (16 scans/s, 4 cm^{-1} resolution) in the wavenumber range of 4500-440 cm^{-1} in KBr pastilles. The morphology and elemental composition of the samples were determined using a Hitachi S-4700 Type II scanning electron microscope (SEM) with a 10 kV accelerating voltage equipped with a Röntec QX2 energy dispersive X-ray spectrometer (EDS). The specific surface area of the materials was analyzed through N_2 sorption by the Brunauer-Emmett-Teller (BET) method with a BELCAT-A. Transmission electron microscopy (TEM) analyses were conducted using 400-mesh copper TEM grids and examined with a Technai G2 20x Twin (Philips/FEI) electron microscopes at an accelerating voltage of 200 kV.

To assess the nickel ion release from Ni-MOF and NiO NPs, the materials were introduced into freshly prepared synthetic wastewater (20 mg/L) and continuously stirred. After 4 and 24 h, the suspensions were centrifuged at 11,000g for 30 min. Subsequently, the supernatant was decanted, and the concentration of Ni ions was determined via Inductively Coupled Plasma-Optical Emission Spectrometry (ICP-OES) using a PerkinElmer Optima 7000 DV.

2.2. Configuration of AGS and AB-AGS bioreactors

The urban wastewater treatment plant in Szeged, Hungary, provided the activated sludge (AS). Aerobic granules were cultivated in two identical sequencing batch reactors (SBRs) with a height-to-diameter ratio of 7 and an effective working volume of 1.4 L. An artificial light source provided 12-h daily illumination near the algal-bacterial AGS SBR at an intensity of approximately 6500 lux, while the AGS reactor was covered by a hood to prevent light exposure. The size of the cultivated granules ranged from 100 to 500 μm.

To ensure oxygenation and complete mixing, air bubbles (superficial air velocity of 2 cm/s) were supplied by diffusers located at the bottom of the reactor. Each cycle involved a decant/feed volume of 50 % of the total volume, with an 8 h hydraulic retention time. The bioreactor operated at 21 ± 3 °C in 4-h cycles, consisting of filling (5 min), aeration (225 min), settling (5 min), and withdrawal (5 min) periods. Peristaltic pumps controlled the filling and withdrawal of wastewater at specified flow rates [37]. Synthetic wastewater (SWW) fed into the reactors consisted of the following components per liter of deionized water: 1200 mg COD as glucose, 110 mg NH_4-N as NH_4Cl, 20 mg PO_4-P added as KH_2PO_4, 200 mg $NaHCO_3$, 25 mg $CaCl_2$, 45 mg $MgSO_4$, and 1 mL of trace element solution (5 mg H_3BO_4, 15 mg $FeSO_4{\cdot}7H_2O$, 6 mg $ZnSO_4{\cdot}7H_2O$, 8 mg $MnSO_4{\cdot}H_2O$, 1.5 mg $CuSO_4{\cdot}5H_2O$, 0.5 mg $CoCl_2{\cdot}6H_2O$, and 0.4 mg MoO_3) [56]. In each experimental setup, the AGS SBRs and AB-AGS PSBRs contained 5.8 g/L of mixed liquor suspended solids (MLSS) and were supplied with Ni-MOF and NiO NP-contaminated SWW at varying concentrations (1, 5, 10, 50, 100, 200 mg/L Ni-MOF and NiO NP). However, the exact amount of nickel was 0.79, 3.93, 7.86, 39.29, 78.58, and 157.16 mg/L for NiO NPs, while for Ni-MOF was 0.27, 1.33, 2.66, 13.29, 26.57, and 53.14 mg/L. The effects of the investigated Ni-based materials were measured over one day (6 cycles for each experiment).

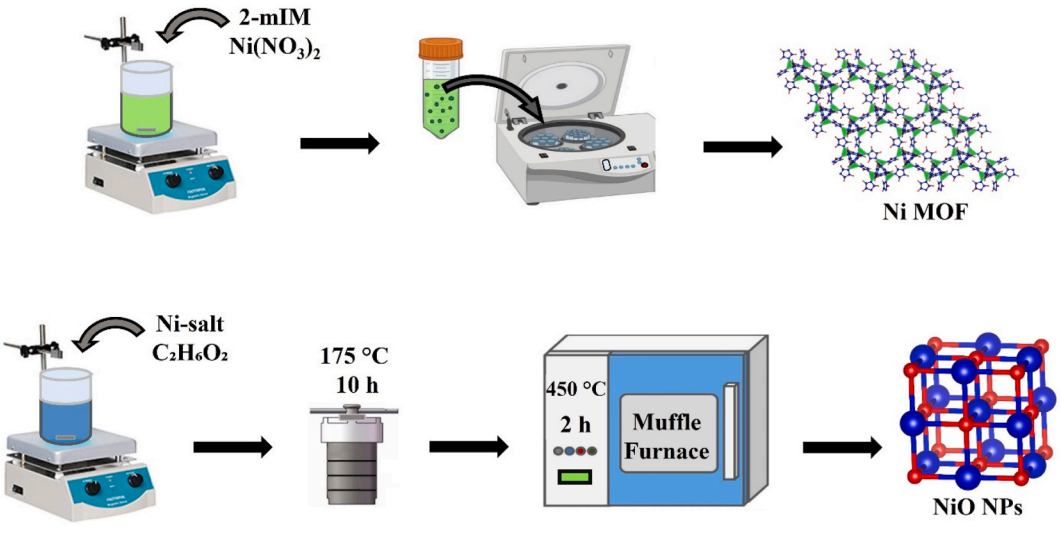

Fig. 1. Schematic illustration of the synthesis process for nickel metal-organic frameworks (Ni-MOF) and nickel oxide nanoparticles (NiO NPs).

2.3. Analytical methods

The effluent water was analyzed for ammonia-nitrogen (NH_4-N), nitrite- and nitrate-nitrogen (NO_2-N and NO_3-N), and total phosphorus (TP) after each cycle (with 6 measurements per experiment). The analysis was conducted using HACH kits and a Hach-Lange DR5000 ultraviolet–visible spectrophotometer. To elucidate the nutrient removal mechanisms of AGS and AB-AGS, we measured the specific oxygen uptake rate (SOUR), specific ammonia uptake rate (SAUR), specific nitrite uptake rate (SNUR), and specific phosphorus uptake rate (SPUR) at the end of each phase, as documented in the Supporting *Information* [37].

Simultaneously, we measured various parameters, including mixed liquor suspended solids (MLSS), the concentration of mixed liquor volatile suspended solids (MLVSS), and settleability (sludge volume index after 5 min of sedimentation-SVI_5). These parameters were analyzed following standard methods [50]. Extracellular polymeric substances (EPS) from both types of granular sludge were extracted using a modified heating method [57]. Protein and polysaccharide (PN and PS) levels in the extracted polymeric substances were assessed using the Anthrone and modified Lowry methods [58]. Granular sludge samples were washed three times with 0.1 M phosphate buffer and then subjected to freeze-drying. The resulting dry granules were examined using SEM to investigate morphological and structural changes.

2.4. Statistical analysis

The experiments were performed in triplicate, and the data are presented as the mean ± standard deviation (SD). A one-way analysis of variance (ANOVA) was applied to evaluate the statistical significance of the results, with a 5 % significance threshold for all analyses.

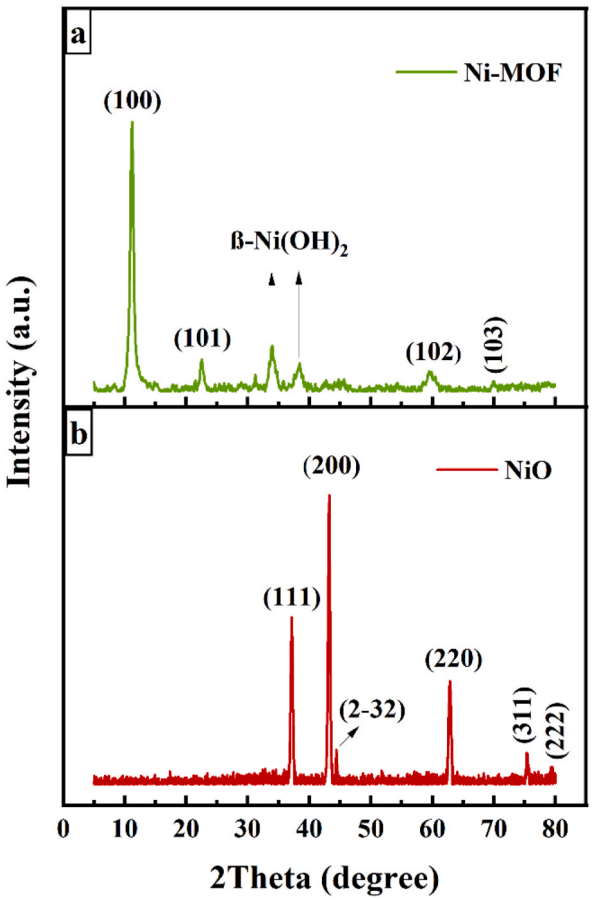

Fig. 2. X-ray diffraction (XRD) patterns of the studied **a)** Nickel metal-organic frameworks (Ni-MOF) and **b)** Nickel oxide nanoparticles (NiO NPs).

3. Results and discussion

3.1. Characterization of Ni-MOF and NiO NPs

XRD was employed to assess the crystalline structure and phase purity of the as-synthesized compounds. Typical XRD patterns of the synthesized Ni-MOF and NiO NPs are shown in Fig. 2. The pure face-centered cubic (FCC) NiO phase can be identified (JCPDS, No. 04–0835) [59], and reflections corresponding to the (111), (200), (220), (311), and (222) crystal planes of bulk NiO were found at 2Theta = 37.13°, 43.26°, 62.86°, 75.39°, and 79.41° (Fig. 2b), respectively [60]. A peak of nickel nitrate (2-32) was detected at 44.50°, suggesting incomplete combustion. An additional 2-h calcination at 450 °C yielded pure cubic NiO nanoparticles [61]. As seen in Fig. 2a, Ni-MOF displays distinct peaks at 11.01°, 22.38°, 59.88°, and 70.05°, which correspond to the (100), (101), (102), and (103) lattice planes, respectively. The (100) plane of Ni-MOF is recognized as the primary exposed facet, and the peaks observed at 33.89° and 38.45° are attributed to the (100) and (101) planes of β-$Ni(OH)_2$ [62–64]. The lattice constant was also calculated from the XRD data. The cubic crystal structure in the space group Fm3m for the (200) crystalline plane has a lattice constant (α) of approximately 4.17 Å for NiO NPs, while the 2-methylimidazolate linker, which forms the ZIF-8 cubic framework, has a lattice constant of 16.91 Å and belongs to the $I\,\bar{4}3\,m$ space group [65,66].

The morphology and chemical composition of the as-synthesized Ni-MOF and NiO NPs were investigated using SEM and EDS and the results are depicted in Fig. 3. Ni-MOF consists of loosely packed 2D nanosheets with an irregular globular morphology, while the NiO sample contains spherical nanoparticles with nearly uniform size distribution. The presence of Ni was verified by EDS in every sample, as shown in the EDS spectra in Fig. 3c and d, along with the approximate atomic percentages of each consisting element. The carbon signal in the NiO spectrum mainly originates from the carbon-based sample holder [67,68].

The Raman spectra of the as-synthesized Ni-MOF and NiO are displayed in Figs. S1a–b. The C-C stretching and C-H bending modes of the imidazole ring in 2-mIM are responsible for the distinctive vibrational peaks at 1042 and 1131 cm^{-1} in the Ni-MOF spectrum, respectively [69]. Additional bands appear at 1353, 1402, and 1494 cm^{-1}, corresponding to the symmetric and asymmetric stretching modes of the carboxylate group [70], while the stretching mode of the benzene ring appears at 1605 cm^{-1} [71]. NiO exhibits prohibited phonon scattering, with first-order and second-order scatterings are responsible for the peaks below and above 600 cm^{-1}, respectively (Fig. S1b). The band at 87 cm^{-1} corresponds to 1-phonon scattering, while the band at 1087 cm^{-1} originates from the 2p:2LO modes of second-order phonon scattering [72].

FT-IR analysis is used to investigate surface interactions during potential nanoparticle adsorption and to identify the structure of adsorbed molecules. The FT-IR spectra of Ni-MOF and NiO NPs, measured between 440 and 4500 cm^{-1}, are shown in Fig. S2. Surface -OH stretching vibrations are responsible for the broad band in 3045 and 3665 cm^{-1}. The Ni-O-Ni stretching mode is responsible for the bands at 1050 cm^{-1} and 576 cm^{-1}, indicating the formation of NiO [73]. The band at 2360 cm^{-1} from the chemically adsorbed CO_2 on the NiO surface and it is also possible to detect the peaks of unaffected C=C bonding at 1720 cm^{-1} and C=O stretching

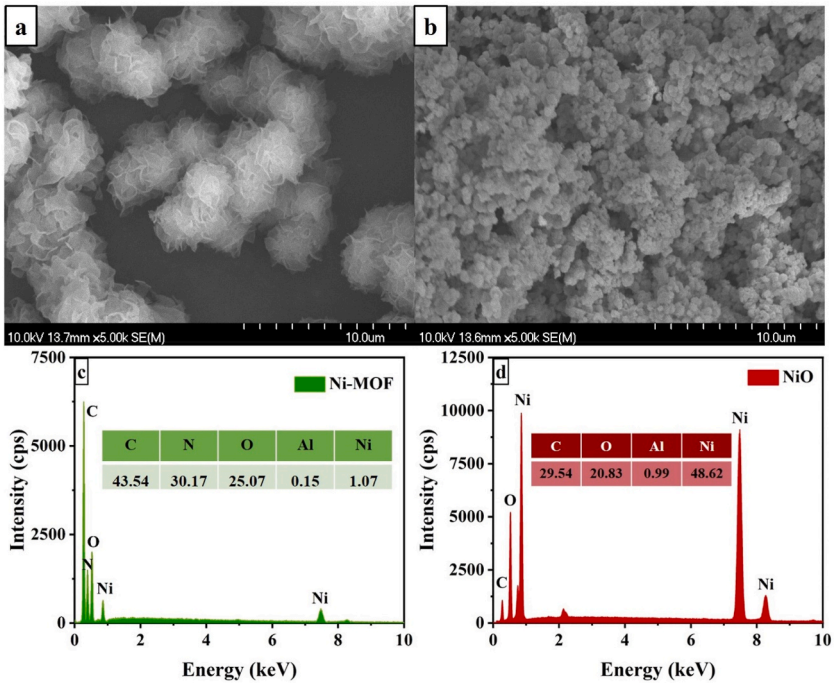

Fig. 3. Scanning electron microscope (SEM) images of **a)** Nickel metal-organic frameworks (Ni-MOF) and **b)** Nickel oxide nanoparticles (NiO NPs), and Energy dispersive X-ray spectrometer (EDS) spectra of **c)** Ni-MOF and **d)** NiO NPs.

carbonyl–carboxyl groups at 1630 cm^{-1} [74]. The symmetric (1477 and 1381 cm^{-1}) and asymmetric (1571 cm^{-1}) stretching vibrations of COO-, stretching vibrations of C-N (1104 cm^{-1}), and the aromatic C-H stretching vibration (755 cm^{-1}) are observed in the Ni-MOF spectrum [75,76]. Additionally, Ni-O stretching accounts for the minor peak observed at 466 cm^{-1} [77]. Nitrogen adsorption-desorption analyses were conducted on the as-prepared Ni-MOF and NiO NP samples to evaluate the Brunauer-Emmett-Teller (BET) specific surface area, total pore volume, and average pore size. It was determined that the specific surface area of NiO NPs was higher by 3 m^2/g than that of the Ni-MOF sample, due to the significantly smaller size and homogeneous distribution of NiO NPs. The calculated values of surface and pore properties are shown in Table S1.

The structural features of Ni-MOF and NiO NPs were examined in further detail using HR-TEM (Fig. S3 a and c) and selected area electron diffraction (SAED) (Fig. S3 b and d). Fig. S3a shows a transparent sample, indicating the thin, layer-like, wrinkled nanostructure of Ni-MOF. The SAED pattern contained two rings with different radii corresponding to the (100) and (101) lattice planes of Ni-MOF. The distinct diffraction rings and lattice fringes of Ni-MOF in the HR-TEM image were barely visible, as observed in previously published literature [78]; this could be due to the inherent structural features of Ni-MOF. TEM image of NiO NPs is shown in Fig. S3c, displaying uniformly sized nanoparticles randomly dispersed on the surface. According to the related HR-TEM image, the majority of the nanoparticles are spheroidal, with an average diameter of 21 $\pm$ 2 nm. The findings indicate that homogenous nanoparticles with a narrow particle size distribution are produced through the facile two-step process. Fig. S3d shows the corresponding SAED pattern for NiO NPs, which displays ring diffraction patterns, indicating the polycrystalline structure of the NiO NPs. The four primary diffraction rings closely match the (111), (200), (220), and (311) planes of the cubic NiO NPs phase based on the indexed diffraction pattern [79].

3.2. *Effect of Ni-MOF and NiO NPs on sludge properties and on bioreactors performance*

Each experiment began with freshly collected AGS and AB-AGS. To obtain directly comparable results for the two wastewater

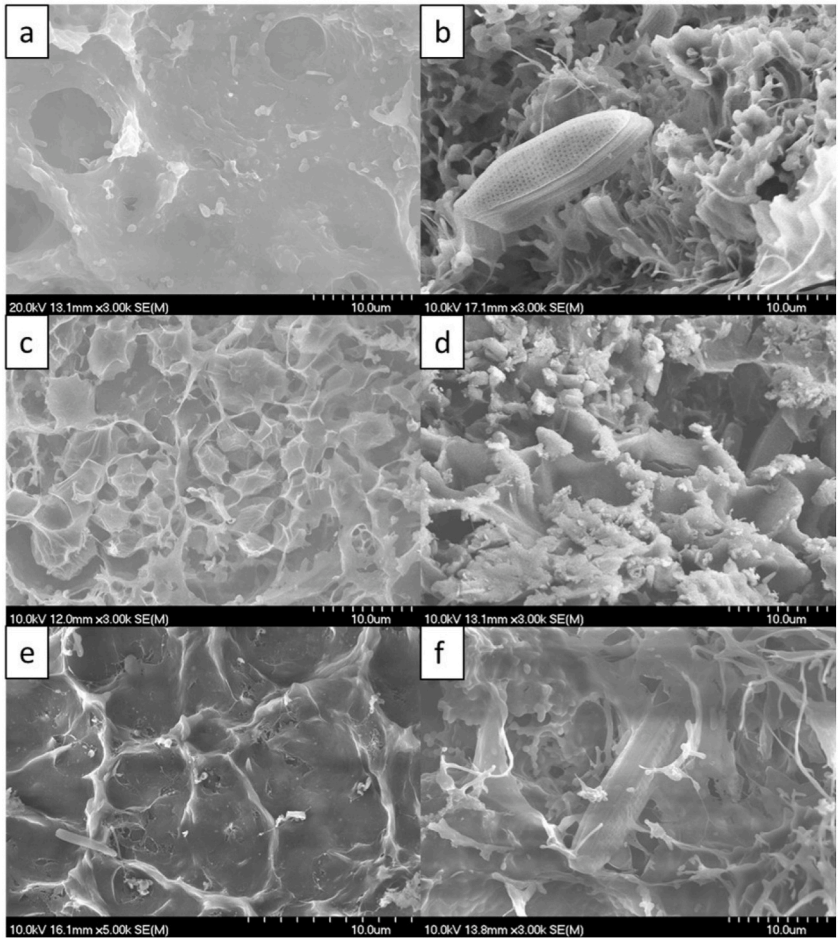

Fig. 4. Scanning electron microscope (SEM) images of aerobic granular sludge (AGS) and algal-bacterial aerobic granular sludge (AB-AGS). The surface of the **a)** aerobic granular sludge, and of the **b)** algal-bacterial granular sludge. The exterior of the **c)** AGS and **d)** AB-AGS after the addition of 200 mg/L nickel metal-organic frameworks (Ni-MOF). The interface of **e)** AGS and **f)** AB-AGS after the exposure of 200 mg/L nickel oxide nanoparticles (NiO NPs).

treatment methods, an average MLSS content and SVI_5 of 5.9 ± 0.1 g/L and 29 mL/g were used in both cases. AGS had a compact and dense structure, with an average size of 500 μm and many bacteria embedded in the polymer matrix. Additionally, channels were observed on the surface of EPS, through which nutrients could penetrate to the anaerobic microorganisms inside the granules (Fig. 4a). In contrast, AB-AGS exhibited a different surface structure, with various types of algae observed on the surface of the granular sludge (Fig. 4b).

The concentrations of NH_4-N, NO_2-N, NO_3-N, and TP in the effluent water from AGS were 0.11 ± 0.02, 0.09 ± 0.02, 0.23 ± 0.04, and 0.71 ± 0.08 mg/L, respectively, while the corresponding concentrations for AB-AGS were 0.04 ± 0.01, 0.02 ± 0.01, 0.09 ± 0.01, and 0.35 ± 0.03 mg/L. The addition of 1, 5, and 10 mg/L Ni-MOF did not adversely affect the performance of the bioreactors; however, increasing concentrations led to a decrease in wastewater treatment efficiency. Additionally, the concentration of nitrate in the effluent water remained stable, indicating that the denitrification processes were unaffected. This phenomenon could be attributed to the shielding effect of EPS surrounding the microbial community [80]. Denitrifying bacteria thrive in predominantly anoxic or facultative anaerobic conditions and are primarily situated within the granules [81]. This provides them with shielding against nickel exposure, preventing heavy metals from permeating the granular structure and inducing adverse effects within the interior of the granules. Previous studies have also reported similar results for AGS and AB-AGS, where the addition of TiO_2 NPs, Ag NPs, and CuO NPs at

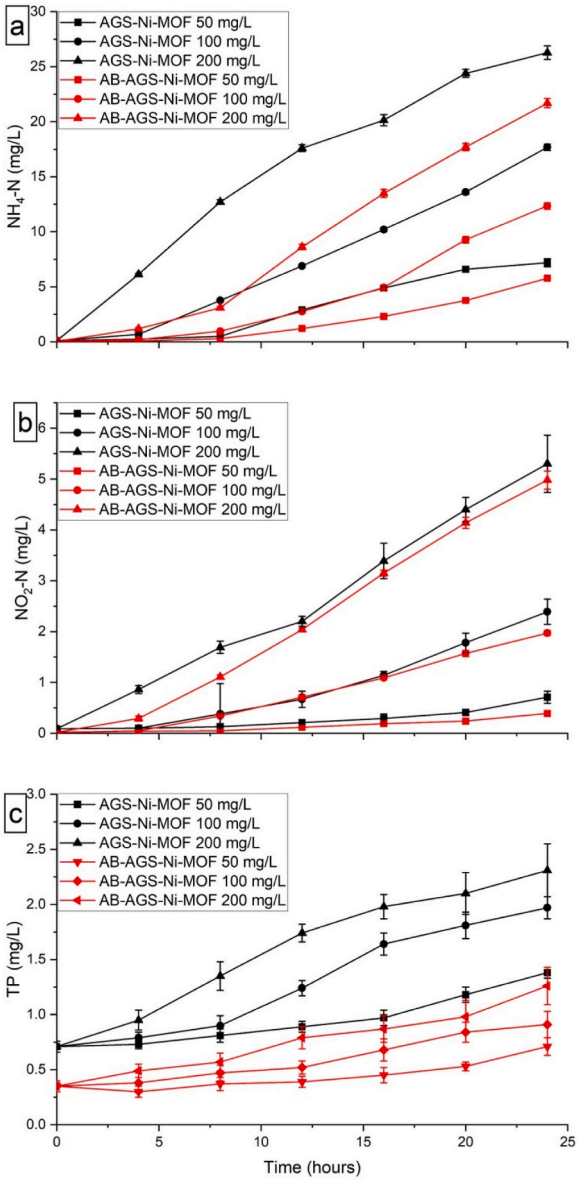

Fig. 5. Effect of nickel metal-organic frameworks (Ni-MOF) on the effluent composition in aerobic granular sludge (AGS) and algal-bacterial aerobic granular sludge (AB-AGS) bioreactors. **a)** ammonia-nitrogen (NH_4-N); **b)** nitrite-nitrogen (NO_2-N); **c)** total phosphorus (TP) contents.

concentrations of 5–30 mg/L maintained stable denitrification processes. However, upon increasing NP concentration to 50 mg/L, a considerably low removal efficiency (5–8%) was observed [48,50,52].

After the introduction of 50 mg/L Ni-MOF into AGS and AB-AGS, the concentration of ammonia in the effluent wastewater increased from 0.11 mg/L and 0.04 mg/L to 7.18 mg/L and 5.78 mg/L, respectively (Fig. 5a). A further increase in Ni-MOF content gradually lowered the removal efficiency. When the Ni-MOF concentration in the influent wastewater was increased to 100 mg/L and 200 mg/L, the ammonia removal rate in SBR and PSBR decreased by 85.3 % and 78.1 %, and to 89.7 % and 81.9 % after 24 h, respectively. The concentration of nitrite slightly increased to 0.71 mg/L and 0.39 mg/L in the case of AGS and AB-AGS after the addition of 50 mg/L Ni-MOF (Fig. 5b). Further increase in the Ni-MOF concentration (100 mg/L) elevated the nitrite amount to 2.39 mg/L and 1.97 mg/L, which then reached 5.3 mg/L and 4.98 mg/L at 200 mg/L Ni-MOF in the two studied systems.

The results also indicate that microorganisms tolerated nickel addition at 50 and 100 mg/L over two cycles, while AB-AGS SBR was more tolerant to contamination. Ma et al. [82] reported that nitrogen removal was negatively affected by nickel stress in activated sludge during wastewater treatment, with a more severe impact observed as the ammonia removal efficiency decreased to 72 % at a 30 mg/L Ni concentration. The results suggest that granulated sludge is more tolerant to toxic nickel than activated sludge, and algal-bacterial granulated sludge demonstrated greater resilience than aerobic granular sludge. Previous studies suggested that this may partly stems from the higher uncontaminated AB-AGS bioreactor performance [83,84], while AB-AGS may demonstrate a symbiotic relationship to shield against nickel exposure [53].

As shown in Fig. 5c, the total phosphorus concentration in the effluent increased in both bioreactors due to the presence of Ni-MOF. Most notably, AB-AGS was more tolerant to nickel than AGS, as Ni-MOF was less toxic at 200 mg/L in the photo-sequencing bioreactor compared to AGS after the addition of 50 mg/L nickel. The TP concentration in the effluent was 1.26 mg/L in AB-AGS at 200 mg/L Ni-MOF, while it was 1.38 mg/L in AGS at 50 mg/L Ni-MOF. At the highest investigated Ni-MOF concentration, the removal efficiency dropped from 96.5 % to 98.3 %–88.5 % and 93.7 % in AGS and AB-AGS, respectively. As their name suggests, during wastewater treatment aerobic polyphosphate-accumulating organisms (PAOs) accumulate phosphorus on their surfaces. Various substances, such as ammonia and nitrite (or free nitrous acid), inhibit PAO activity, making them highly sensitive to these pollutants [52,56,85]. In the

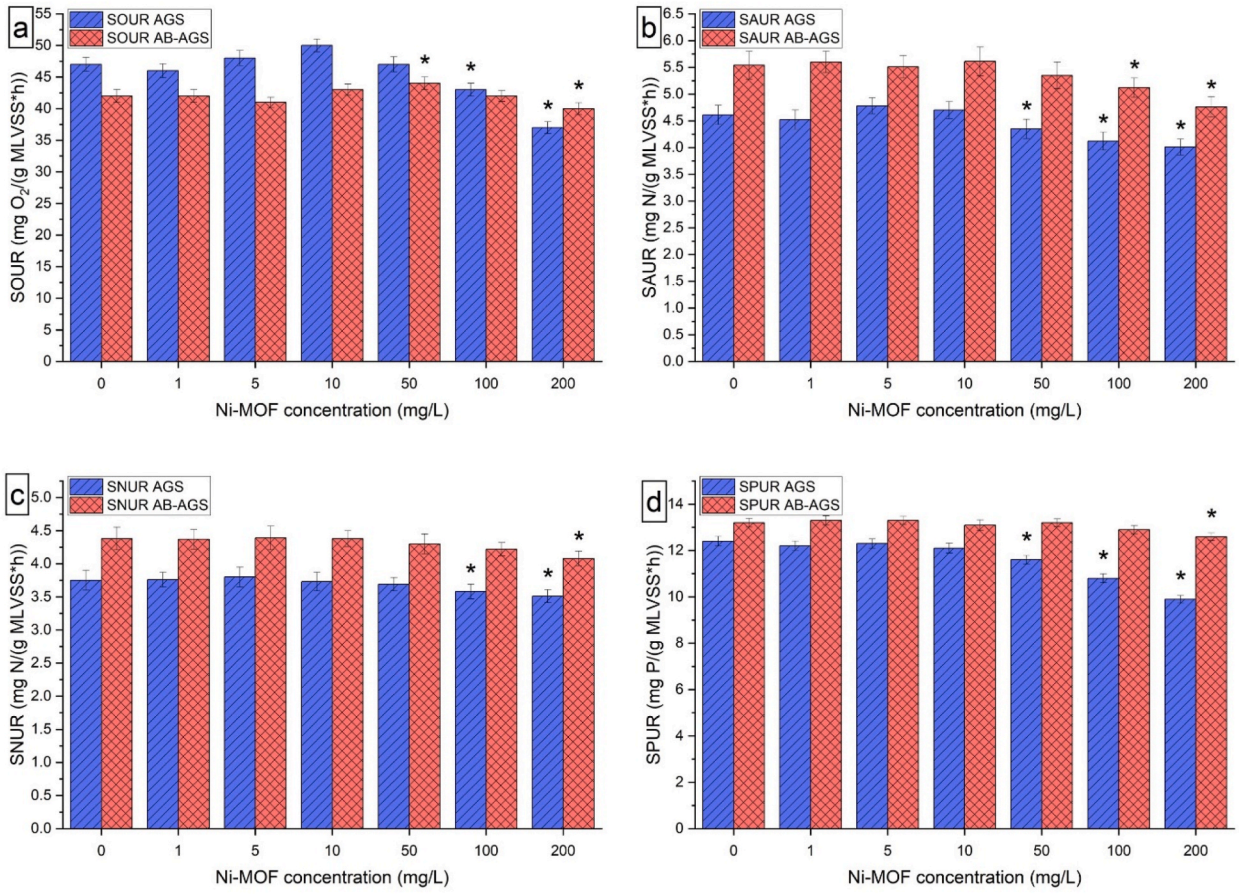

Fig. 6. Impacts of nickel metal-organic frameworks (Ni-MOF) and nickel oxide nanoparticles (NiO NPs) on the microbial activities of aerobic granular sludge (AGS) and algal-bacterial aerobic granular sludge (AB-AGS). **a)** specific oxygen uptake rate (SOUR); **b)** specific ammonia uptake rate (SAUR); **c)** specific nitrite uptake rate (SNUR); **d)** specific phosphorus uptake rate (SPUR). The stars show statistical differences (* = $p < 0.05$) compared to the control (without Ni-MOF or NiO NPs; one-way ANOVA).

studied bioreactors, especially in AGS, the concentrations of ammonia and nitrite increased with increasing Ni-MOF concentrations. This suggests that the combined effect of these three substances may inhibit phosphorus removal. The higher resilience of AB-AGS against nickel suggests that algae play an important role in phosphate removal, along with a better tolerance to Ni [84]. The dissimilarity in Ni-MOF tolerance could arise from its different effect on the microorganisms, which leads to the secretion of EPSs. As shown in Fig. 4c, the contiguous polymer matrix on the surface of the aerobic granules underwent noticeable changes, which were also observed on the exterior of the algal-bacterial sludge (Fig. 4d). However, compared to the initial sludge, the algae were not merely attached to the surface, but were embedded in the EPS matrix. Consequently, the algae were protected from nickel and retained their nutrient removal ability.

The addition of NiO NPs did not influence the bioreactors' performance, as the removal of NH_4-N, NO_2-N, NO_3-N, and TP remained stable. This could be due to the lower solubility of NiO NPs compared to Ni-MOF in water. In the solubility tests, 59.4 % and 98.4 % of the nickel from Ni-MOF was detected in water after 4 and 24 h, respectively, whereas nickel was not detectable in the case of NiO NPs. Consequently, NiO NPs attached to the polymer matrix without inducing any negative effects on the microorganisms (Fig. 4e–f, and Figs. S4a–b). Wang et al. [33] demonstrated a decline in nutrient removal efficiency in activated sludge at 10 mg/L of NiO NPs, accompanied by an increase in Ni concentration in the effluent water. Similarly, Xiao et al. [28] reported inhibited nutrient removal even at 0.1 mg/L of NiO NPs after long-term exposure. These results suggest that AGS and AB-AGS systems represent promising alternatives to the CAS process. Both AGS and AB-AGS have exhibited excellent simultaneous removal of carbon, nitrogen, and phosphorus, making them viable alternatives to CAS technology, particularly for treating contaminated wastewater.

3.3. Effect of Ni-MOF and NiO NPs on the microbial activity of AGS and AB-AGS

Fig. 6 illustrates the effect of Ni-MOF on the microbial activity of aerobic granular and algal-bacterial granular sludge. In the initial sludge, the specific oxygen uptake rates (SOUR) were 47 and 42 mg O_2/(g MLVSS*h) for AGS and AB-AGS, respectively. The addition of 1, 5, and 10 mg/L Ni-MOF to the AGS bioreactors had a positive effect on SOUR, whereas in AB-AGS we observed a significant increase ($p < 0.05$) in microbial activity, with the maximum observed at 50 mg/L nickel concentration (Fig. 6a). This suggests that nickel positively affects the activity of heterotrophic microorganisms up to a certain concentration. Previous studies have reported similar observations, where the oxygen uptake rate of the granules increased upon addition of graphene oxide nanoparticles or by increasing the salinity of wastewater [37,86]. However, increasing Ni-MOF concentration to 100 and 200 mg/L significantly decreased the SOUR in both types of sludge. At the highest investigated Ni-MOF concentration, the SOUR significantly decreased to 37 and 40 mg O_2/(g MLVSS*h) in AGS and AB-AGS, respectively ($p < 0.05$). However, the results show higher nickel tolerance in the heterotrophic microorganisms responsible for degrading organic matter in the algal-bacterial sludge. Another difference between the two types of sludge is the lower SOUR of AB-AGS, which can be explained by the absence of sunlight during the measurements, leading to decreased bioactivity of the photoautotrophic algae [85].

Ni-MOF positively affected the specific ammonia uptake rate (SAUR) in both systems up to 10 mg/L, but it dropped with the addition of ≥50 mg/L Ni (Fig. 6b). A similar phenomenon was observed in the specific nitrite uptake rate (SNUR) as well, indicating that >50 mg/L Ni-MOF negatively affects the microbial activity of ammonia- and nitrite-oxidizing microorganisms (AOB and NOB) (Fig. 6c). These observations may explain the reduced ammonia and nitrite removal rates in the bioreactors. When the SAUR and SNUR values equaled those in the initial granulated sludge, no increase in ammonia or nitrite content was found in the effluent wastewater. In contrast, when the concentration of Ni-MOF was 50, 100, or 200 mg/L in AGS, both microbial activities began to decline significantly, leading to increased nitrogen content in the effluent wastewater. However, a significant decrease in SAUR and SNUR in AB-AGS was observed only at 200 mg/L Ni-MOF, which may explain the better nitrogen removal efficiencies compared to AGS. These observations have also been reported in previous studies, where changes in SAUR and SNUR were highly correlated with the ammonia and nitrite concentrations in the effluent [86,87]. At the highest Ni-MOF concentration, the SAUR and SNUR decreased compared to the initial sludge by 13.02 % and 14.08 % in the AGS, and only by 6.41 % and 6.85 % in the AB-AGS, respectively. This suggests that the presence of algae enhances the bioactivity of AOB and NOB.

The specific phosphorus uptake rate (SPUR) in the AGS and AB-AGS was 12.4 and 13.2 mg P/(g MLVSS*h), respectively, in the initial phase (Fig. 6d). The presence of 10 mg/L Ni-MOF decreased the SPUR in AGS, which significantly dropped by 20.18 % to 9.91 mg P/(g MLVSS*h) at 200 mg/L Ni-MOF. These results explain the high levels of TP in the effluent wastewater. Nickel negatively affected the aerobic phosphate-accumulating organisms, reducing their metabolic activity and ultimately leading to phosphorus release into the effluent. Previous investigations have observed similar effects, where a decreased phosphorus uptake rate led to a decline in phosphate removal rate with increasing concentrations of Zn, Ce, and Ag [87–89]. However, only a slight drop of 2.28 % was found in SPUR in the AB-AGS with 100 mg/L Ni-MOF, while a significant decrease was seen after 200 mg/L Ni-MOF addition (SPUR decreased from 13.2 to 12.6 mg P/(g MLVSS*h)), respectively. These observations align well with the water chemistry results, as slight decrease in microbial activity only led to a mild increase in total phosphorus in the effluent. The relatively stable SPUR can be attributed to i) the high phosphorus uptake ability of algae [90], ii) their higher tolerance to heavy metals [91], and iii) the fact that algae were embedded in the EPS matrix (Fig. 4d), providing them with protection from nickel.

3.4. Effects of Ni-MOF and NiO NPs on EPS contents of AGS and AB-AGS

Extracellular polymeric substances (EPSs) form a complex polymer matrix that enhance sludge aggregation, shield bacteria from adverse shocks, supplies nutrients to the cells, and adsorbs various inorganic compounds [51]. The initial content of EPS, polysaccharides (PS), and proteins (PN) was 109, 46, and 63 mg/g MLVSS in AGS, and 127, 52, and 75 mg/g MLVSS in the algal-bacterial

sludge, respectively (Fig. 7). It is evident that the algal-bacterial sludge contains more polymer substances with a higher PN/PS ratio, consistent with observations from previous studies [84,85]. The EPS content increased in both types of sludge after the addition of 1, 5, and 10 mg/L Ni-MOF, which may explain the stable nutrient removal rates. At 10 mg/L Ni-MOF, the EPS content was significantly elevated in the granular and algal-bacterial sludges to reaching 148 and 157 mg/g MLVSS, respectively (Fig. 7a and b). While the PN content increased to 95 and 97 mg/g MLVSS, the PN/PS ratio in the polymer rose to 1.79 and 1.61, respectively. Zheng et al. [92] reported similar findings after the addition of CeO_2 to granulated sludge. This was attributed to the induction of heat shock-like proteins in response to toxic substances.

However, further increases in the amount of metal-organic framework caused a decline in polymer content. When the Ni-MOF concentration reached 100 and 200 mg/L, the EPS content, primarily PN, was lower compared to that in the initial sludge, resulting in a depressed PN/PS ratio. The EPS content in AGS significantly declined to 97.1 and 89.2 mg/g MLVSS at 100 and 200 mg/L Ni-MOF, while in AB-AGS the EPS decreased significantly to 102.9 mg/g MLVSS only after exposure to 200 mg/L Ni-MOF. These observations also correlate well with water chemistry results, suggesting that the overproduction of polymer substances, particularly proteins, served as a defense mechanism for microorganisms to withstand harmful chemicals [93]. Similar observations have been reported in other studies, where ZnO, TiO_2, and CuO were introduced to AGS and AB-AGS at somewhat lower concentrations (1–10 mg/L). As a result, higher EPS production was observed, maintaining stable wastewater treatment. However, a further increase in metal concentration ($\geq$30 mg/L) inhibited polymer matrix secretion, and water treatment efficiency decreased [50,52,53,94].

At 1, 5, 10, and 50 mg/L NiO NP contents the EPS in both sludges remained stable, leading to the conclusion that nanoparticles did not cause any discernible negative or positive effects on wastewater treatment processes up to 50 mg/L (Fig. 7c and d). However, at higher concentrations (100 and 200 mg/L), we observed a significant increase in EPS content, although the PS remained stable (49-54 mg/g MLVSS). PN and the PN/PS ratio increased to 91 mg/g MLVSS and 1.82 in the granulated sludge, and to 114 mg/g MLVSS and 2.11 in the algal-bacterial sludge, respectively. These findings show that NiO NPs had a mild negative effect at concentrations of $\geq$100

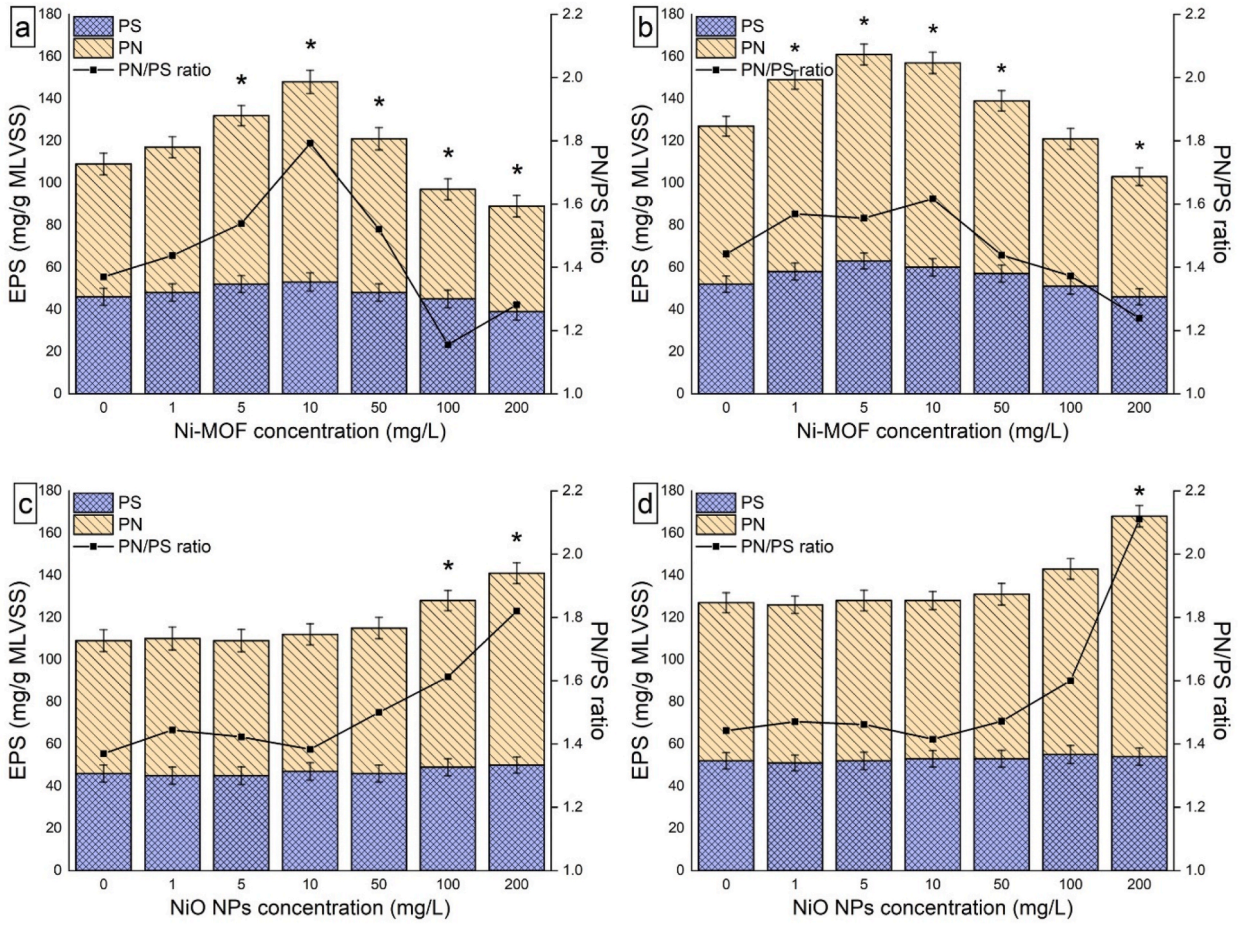

Fig. 7. Change in extracellular polymeric substances (EPS) (sum of polysaccharide (PS) and protein (PN)) after addition of nickel metal-organic frameworks (Ni-MOF) and nickel oxide nanoparticles (NiO NPs). **a)** EPS content in aerobic granular sludge (AGS) after addition of Ni-MOF; **b)** EPS content in algal-bacterial aerobic granular sludge (AB-AGS) after addition of Ni-MOF; **c)** EPS content in AGS after addition of NiO NPs; **d)** EPS content in AB-AGS after addition of NiO NPs. The stars show statistical differences (* = $p < 0.05$) compared to the control (without Ni-MOF or NiO NPs; one-way ANOVA).

mg/L. However, the microorganisms in the sludge, as a defense mechanism, secreted more EPS and adapted to the new environment [48], thereby enabling AGS and AB-AGS to effectively treat wastewater containing NiO NPs.

4. Conclusions

In this study, the impacts of Ni-MOF and NiO NPs (at concentrations ranging from 1 to 200 mg/L) on the performance of AGS and AB-AGS were investigated. The bioreactors tolerated Ni-MOF concentrations below 10 mg/L, but at concentrations above 50 mg/L, the removal efficiency of NH_4-N, NO_2-N, and TP declined. However, Ni-MOF had a lesser negative effect on nutrient removal and microbial activity in AB-AGS, attributed to the higher amount of EPS, within which the algae were embedded, suggesting a strong symbiotic relationship between algae and bacteria. The efficiency of wastewater treatment remained unaffected by the addition of NiO NPs, even at 200 mg/L, likely due to their insolubility. While the results provide valuable insights into the effects of Ni-MOF and NiO NPs on AGS and AB-AGS, the study is limited by the short-term nature of the experiments and the controlled laboratory conditions. Future studies should focus on molecular biology investigations to elucidate microbial responses to Ni-MOF and NiO NPs, evaluate the long-term impacts of these materials on wastewater treatment performance, explore the impact of real wastewater conditions, and further optimize the algal-bacterial symbiosis to enhance resilience against metal contaminants. Additionally, future research should explore the use of green nanomaterials as a sustainable alternative, assessing their efficacy and potential environmental benefits in wastewater treatment applications.

CRediT authorship contribution statement

Alfonz Kedves: Writing – original draft, Visualization, Validation, Software, Methodology, Investigation, Formal analysis, Data curation, Conceptualization. **Çağdaş Yavuz:** Writing – original draft, Visualization, Software, Methodology, Investigation, Formal analysis, Data curation. **Orsolya Kedves:** Visualization, Software, Methodology, Investigation, Formal analysis. **Henrik Haspel:** Writing – review & editing, Supervision, Resources, Project administration, Funding acquisition, Formal analysis. **Zoltán Kónya:** Writing – review & editing, Supervision, Resources, Project administration, Funding acquisition, Formal analysis.

Data and code availability statement

Data will be made available on request.

Ethics declaration

Review and/or approval by an ethics committee as well as informed consent was not required for this study because this article did not involve any direct experimentation/studies on living beings.

Declaration of competing interest

The authors declare that they have no known competing financial interests or personal relationships that could have appeared to influence the work reported in this paper.

Acknowledgment

O.K. acknowledges financial support of the New National Excellence Program of the Ministry for Culture and Innovation from the source of the National Research, Development and Innovation Fund (ÚNKP-23-4-SZTE-556).

H.H. acknowledges financial support of the János Bolyai Research Grant of the Hungarian Academy of Sciences (BO/682/22) and the New National Excellence Program of the Ministry for Culture and Innovation from NKFI Fund (ÚNKP-22-5-SZTE-574). Project no. RRF-2.3.1-21-2022-00009 (National Laboratory for Renewable Energy) has been implemented with the support provided by the Recovery and Resilience Facility of the European Union within the framework of Programme Széchenyi Plan Plus. This project has received funding from the HUN-REN Hungarian Research Network.

Z.K. acknowledges financial support of Hungarian Scientific Research Fund (OTKA) K138176 and K135918.

Appendix A. Supplementary data

Supplementary data to this article can be found online at https://doi.org/10.1016/j.heliyon.2024.e40796.

References

[1] M. Taeño, D. Maestre, A. Cremades, An approach to emerging optical and optoelectronic applications based on NiO micro- and nanostructures, Nanophotonics 10 (2021) 1785–1799, https://doi.org/10.1515/nanoph-2021-0041.

[2] D. Di Girolamo, F. Di Giacomo, F. Matteocci, A.G. Marrani, D. Dini, A. Abate, Progress, highlights and perspectives on NiO in perovskite photovoltaics, Chem. Sci. 11 (2020) 7746–7759, https://doi.org/10.1039/d0sc02859b.

[3] G. Zhou, W. Ding, Y. Guan, T. Wang, C. Liu, L. Zhang, J. Yin, Y. Fu, Progress of NiO-based anodes for high-performance Li-ion batteries, Chem. Rec. 22 (2022), https://doi.org/10.1002/tcr.202200111.

[4] W. Fan, X. Wang, X. Liu, B. Xu, X. Zhang, W. Wang, X. Wang, Y. Wang, F. Dai, D. Yuan, D. Sun, Regulating C 2 H 2 and CO 2 storage and separation through pore environment modification in a microporous Ni-MOF, ACS Sustain. Chem. Eng. 7 (2019) 2134–2140, https://doi.org/10.1021/acssuschemeng.8b04783.

[5] S. Chen, X. Li, J. Duan, Y. Fu, Z. Wang, M. Zhu, N. Li, Investigation of highly efficient adsorbent based on Ni-MOF-74 in the separation of CO2 from natural gas, Chem. Eng. J. 419 (2021), https://doi.org/10.1016/j.cej.2021.129653.

[6] K. Song, S. Liang, X. Zhong, M. Wang, X. Mo, X. Lei, Z. Lin, Tailoring the crystal forms of the Ni-MOF catalysts for enhanced photocatalytic CO2-to-CO performance, Appl. Catal. B Environ. 309 (2022) 121232, https://doi.org/10.1016/j.apcatb.2022.121232.

[7] C. Wang, X. Ye, Y. Liu, Z. Jia, C. Cao, Q. Xiao, J. Du, X. Kong, X. Wu, Z. Chen, Y. Xi, Enhanced anaerobic digestion for degradation of swine wastewater through a Fe/Ni-MOF modified microbial electrolysis cell, J. Clean. Prod. 380 (2022) 134773, https://doi.org/10.1016/j.jclepro.2022.134773.

[8] M. Zeraati, V. Alizadeh, P. Kazemzadeh, M. Safinejad, H. Kazemian, G. Sargazi, A new nickel metal organic framework (Ni-MOF) porous nanostructure as a potential novel electrochemical sensor for detecting glucose, J. Porous Mater. 29 (2022) 257–267, https://doi.org/10.1007/s10934-021-01164-3.

[9] K.O. Otun, S. Zong, D. Hildebrandt, X. Liu, Self-assembled Zn-functionalized Ni-MOF as an efficient electrode for electrochemical energy storage, J. Phys. Chem. Solid. 167 (2022) 110779, https://doi.org/10.1016/j.jpcs.2022.110779.

[10] A.A. Mohammadi, S. Moghanlo, M.S. Kazemi, S. Nazari, S.K. Ghadiri, H.N. Saleh, M. Sillanpää, Comparative removal of hazardous cationic dyes by MOF-5 and modified graphene oxide, Sci. Rep. 12 (2022) 15314, https://doi.org/10.1038/s41598-022-19550-5.

[11] A.A. Mohammadi, Z. Niazi, K. Heidari, A. Afarinandeh, M. Samadi Kazemi, G.A. Haghighat, Y. Vasseghian, S. Rezania, A. Barghi, Nickel and iron-based metal-organic frameworks for removal of organic and inorganic model contaminants, Environ. Res. 212 (2022) 113164, https://doi.org/10.1016/j.envres.2022.113164.

[12] S. Xiong, S. Jiang, J. Wang, H. Lin, M. Lin, S. Weng, S. Liu, Y. Jiao, Y. Xu, J. Chen, A high-performance hybrid supercapacitor with NiO derived NiO@Ni-MOF composite electrodes, Electrochim. Acta 340 (2020) 135956, https://doi.org/10.1016/j.electacta.2020.135956.

[13] A. Afarinandeh, K. Heidari, M. Barczak, M.H. Abdellattif, Z. Izadi Yazdanaabadi, A.A. Mohammadi, G.A. Haghighat, M. Shams, Controlled removal of fluoride by ZIF-8, ZIF-67, and Ni-MOF of different morphologies, Arab. J. Chem. 16 (2023) 104837, https://doi.org/10.1016/j.arabjc.2023.104837.

[14] M. Shams, Z. Niazi, M.R. Saeb, S. Mozaffari Moghadam, A.A. Mohammadi, M. Fattahi, Tailoring the topology of ZIF-67 metal-organic frameworks (MOFs) adsorbents to capture humic acids, Ecotoxicol. Environ. Saf. 269 (2024) 115854, https://doi.org/10.1016/j.ecoenv.2023.115854.

[15] S. Mazloomi, A. Amarloei, F. Gholami, G.A. Haghighat, G. Badalians Gholikandi, H. Nourmoradi, A.A. Mohammadi, M. Fattahi, B. Nguyen Le, Parametric study and process modeling for metronidazole removal by rhombic dodecahedron ZIF-67 crystals, Sci. Rep. 13 (2023) 14654, https://doi.org/10.1038/s41598-023-41724-y.

[16] J.J. Xu, Y.F. Cheng, L.Z.J. Xu, Y.Y. Liu, B.Q. Zhu, N.S. Fan, B.C. Huang, R.C. Jin, The revolution of performance, sludge characteristics and microbial community of anammox biogranules under long-term NiO NPs exposure, Sci. Total Environ. 649 (2019) 440–447, https://doi.org/10.1016/j.scitotenv.2018.08.386.

[17] I.O. Plekhanova, A.P. Zarubina, S.E. Plekhanov, Ecotoxicological assessment of nickel pollution of soil and water environments adjacent to soddy–podzolic soil, Moscow Univ. Soil Sci. Bull. 72 (2017) 71–77, https://doi.org/10.3103/s0147687417020065.

[18] V. Léon, J. Rabier, R. Notonier, R. Barthelémy, X. Moreau, S. Bouraïma-Madjèbi, J. Viano, R. Pineau, Effects of three nickel salts on germinating seeds of Grevillea exul var. rubiginosa, an endemic serpentine proteaceae, Ann. Bot. 95 (2005) 609–618, https://doi.org/10.1093/aob/mci066.

[19] G. Genchi, A. Carocci, G. Lauria, M.S. Sinicropi, A. Catalano, Nickel: human health and environmental toxicology, Int. J. Environ. Res. Publ. Health 17 (2020), https://doi.org/10.3390/ijerph17030679.

[20] P. Raju, T. Ramalingam, T. Nooruddin, S. Natarajan, In vitro assessment of antimicrobial, antibiofilm and larvicidal activities of bioactive nickel metal organic framework, J. Drug Deliv. Sci. Technol. 56 (2020) 101560, https://doi.org/10.1016/j.jddst.2020.101560.

[21] Y. Li, S. Shang, J. Shang, W.X. Wang, Toxicity assessment and underlying mechanisms of multiple metal organic frameworks using the green algae Chlamydomonas reinhardtii model, Environ. Pollut. 291 (2021) 118199, https://doi.org/10.1016/j.envpol.2021.118199.

[22] W. Kamal, R. Mahmoud, A.E. Allah, A.A. Farghali, A. Abdelwahab, D.H.M. Alkhalifah, W.N. Hozzein, M.B.E.D. Mohamed, S.A.A. Abdel Aziz, Controlling multi-drug-resistant traits of Salmonella obtained from retail poultry shops using metal–organic framework (MOF) as a novel technique, Microorganisms 11 (2023), https://doi.org/10.3390/microorganisms11102506.

[23] H.M. Abd El Salam, H.N. Nassar, A.S.A. Khidr, T. Zaki, Antimicrobial activities of green synthesized Ag nanoparticles @ Ni-MOF nanosheets, J. Inorg. Organomet. Polym. Mater. 28 (2018) 2791–2798, https://doi.org/10.1007/s10904-018-0950-4.

[24] Y.W. Baek, Y.J. An, Microbial toxicity of metal oxide nanoparticles (CuO, NiO, ZnO, and Sb2O3) to Escherichia coli, Bacillus subtilis, and Streptococcus aureus, Sci. Total Environ. 409 (2011) 1603–1608, https://doi.org/10.1016/j.scitotenv.2011.01.014.

[25] M. Ates, V. Demir, Z. Arslan, M. Camas, F. Celik, Toxicity of engineered nickel oxide and cobalt oxide nanoparticles to Artemia salina in seawater, Water, Air. Soil Pollut. 227 (2016), https://doi.org/10.1007/s11270-016-2771-9.

[26] M. Faisal, Q. Saquib, A.A. Alatar, A.A. Al-Khedhairy, A.K. Hegazy, J. Musarrat, Phytotoxic hazards of NiO-nanoparticles in tomato: a study on mechanism of cell death, J. Hazard Mater. 250–251 (2013) 318–332, https://doi.org/10.1016/j.jhazmat.2013.01.063.

[27] V. Baskar, N. Safia, K. Sree Preethy, S. Dhivya, M. Thiruvengadam, R. Sathishkumar, A comparative study of phytotoxic effects of metal oxide (CuO, ZnO and NiO) nanoparticles on in-vitro grown Abelmoschus esculentus, Plant Biosyst. 155 (2021) 374–383, https://doi.org/10.1080/11263504.2020.1753843.

[28] J. Xiao, J. Huang, M. Wang, M. Huang, Y. Wang, The fate and long-term toxic effects of NiO nanoparticles at environmental concentration in constructed wetland: enzyme activity, microbial property, metabolic pathway and functional genes, J. Hazard Mater. 413 (2021) 125295, https://doi.org/10.1016/j.jhazmat.2021.125295.

[29] A. Oukarroum, W. Zaidi, M. Samadani, D. Dewez, Toxicity of nickel oxide nanoparticles on a freshwater green algal strain of chlorella vulgaris, BioMed Res. Int. 2017 (2017), https://doi.org/10.1155/2017/9528180.

[30] C.A. Sousa, H.M.V.M. Soares, E.V. Soares, Toxic effects of nickel oxide (NiO) nanoparticles on the freshwater alga Pseudokirchneriella subcapitata, Aquat. Toxicol. 204 (2018) 80–90, https://doi.org/10.1016/j.aquatox.2018.08.022.

[31] A.D. Salunkhe, P.K. Pagare, A.P. Torane, Review on recent modifications in nickel metal-organic framework derived electrode. Ni-MOF) Materials for Supercapacitors, Springer US, 2023, https://doi.org/10.1007/s10904-022-02503-w.

[32] L. Han, J. Ma, H. Lin, C. Chen, J. Teng, B. Li, D. Zhao, Y. Xu, W. Yu, L. Shen, A novel flower-like nickel-metal-organic framework (Ni-MOF) membrane for efficient multi-component pollutants removal by gravity, Chem. Eng. J. 470 (2023), https://doi.org/10.1016/j.cej.2023.144311.

[33] S. Wang, Z. Li, M. Gao, Z. She, L. Guo, D. Zheng, Y. Zhao, B. Ma, F. Gao, X. Wang, Long-term effects of nickel oxide nanoparticles on performance, microbial enzymatic activity, and microbial community of a sequencing batch reactor, Chemosphere 169 (2017) 387–395, https://doi.org/10.1016/j.chemosphere.2016.10.139.

[34] C.-S.S. He, L. Huang, R.-R.R. Ding, H.-Y.Y. Yang, Y.-X.X. Wang, J. Li, Y. Mu, Progressive stress response of the anaerobic granular sludge to nickel nanoparticles: experimental investigations and mathematic modelling, Environ. Sci.: Nano 6 (2019) 1536–1548, https://doi.org/10.1039/C9EN00190E.

[35] M. Zhang, B. Ji, S. Wang, J. Gu, Y. Liu, Granule size informs the characteristics and performance of microalgal-bacterial granular sludge for wastewater treatment, Bioresour. Technol. 346 (2022) 126649, https://doi.org/10.1016/j.biortech.2021.126649.

[36] S. Ren, Assessing wastewater toxicity to activated sludge: recent research and developments, Environ. Int. 30 (2004) 1151–1164, https://doi.org/10.1016/j.envint.2004.06.003.

[37] A. Kedves, A. Rónavári, Z. Kónya, Long-term effect of graphene oxide on the aerobic granular sludge wastewater treatment process, J. Environ. Chem. Eng. 9 (2021) 1–7, https://doi.org/10.1016/j.jece.2020.104853.

[38] X. Chen, J. Wang, Q. Wang, Z. Li, T. Yuan, Z. Lei, Z. Zhang, K. Shimizu, D.J. Lee, A comparative study on simultaneous recovery of phosphorus and alginate-like exopolymers from bacterial and algal-bacterial aerobic granular sludges: effects of organic loading rate, Bioresour. Technol. 357 (2022) 127343, https://doi.org/10.1016/j.biortech.2022.127343.

[39] Y. Zhang, X. Dong, S. Liu, Z. Lei, K. Shimizu, Z. Zhang, Y. Adachi, D.J. Lee, Rapid establishment and stable performance of a new algal-bacterial granule system from conventional bacterial aerobic granular sludge and preliminary analysis of mechanisms involved, J. Water Process Eng. 34 (2020) 101073, https://doi.org/10.1016/j.jwpe.2019.101073.

[40] X. Zheng, Z. Han, X. Shao, Z. Zhao, H. Zhang, T. Lin, S. Yang, C. Zhou, Response of aerobic granular sludge under polyethylene microplastics stress: physicochemical properties, decontamination performance, and microbial community, J. Environ. Manag. 323 (2022) 116215, https://doi.org/10.1016/j.jenvman.2022.116215.

[41] D. Ilmasari, A. Yuniarto, C. Khen, L.D.A. Purba, Z. Lei, A. Yuzir, Microalgal-bacterial aerobic granular sludge for old leachate treatment: development, performance, and lipid production, J. Clean. Prod. 417 (2023) 138053, https://doi.org/10.1016/j.jclepro.2023.138053.

[42] B. Ji, M. Zhang, J. Gu, Y. Ma, Y. Liu, A self-sustaining synergetic microalgal-bacterial granular sludge process towards energy-efficient and environmentally sustainable municipal wastewater treatment, Water Res. 179 (2020) 115884, https://doi.org/10.1016/j.watres.2020.115884.

[43] Y. Wei, M. Ji, R. Li, F. Qin, Organic and nitrogen removal from landfill leachate in aerobic granular sludge sequencing batch reactors, Waste Manag. 32 (2012) 448–455, https://doi.org/10.1016/j.wasman.2011.10.008.

[44] S. Wang, Y. Zhang, H. Ge, H. Hou, H. Zhang, K. Pi, Cultivation of algal-bacterial granular sludge and degradation characteristics of tetracycline, Water Environ. Res. 95 (2023) 1–10, https://doi.org/10.1002/wer.10846.

[45] B. Zhang, Y. He, W. Shi, L. Liu, L. Li, C. Liu, P.N.L. Lens, Biotransformation of sulfamethoxazole (SMX) by aerobic granular sludge: removal performance, degradation mechanism and microbial response, Sci. Total Environ. 858 (2023) 159771, https://doi.org/10.1016/j.scitotenv.2022.159771.

[46] J. Zou, J. Yang, H. He, X. Wang, R. Mei, L. Cai, J. Li, Effect of seed sludge type on aerobic granulation, pollutant removal and microbial community in a sequencing batch reactor treating real textile wastewater, Int. J. Environ. Res. Publ. Health 19 (2022), https://doi.org/10.3390/ijerph191710940.

[47] C. Lin, P. Cao, X. Xu, B. Ye, Algal-bacterial symbiosis system treating high-load printing and dyeing wastewater, continuous-flow reactors under natural light, Water (Switzerland) 11 (2019), https://doi.org/10.3390/w11030469.

[48] X. Quan, Y. Cen, F. Lu, L. Gu, J. Ma, Response of aerobic granular sludge to the long-term presence to nanosilver in sequencing batch reactors: reactor performance, sludge property, microbial activity and community, Sci. Total Environ. 506–507 (2015) 226–233, https://doi.org/10.1016/j.scitotenv.2014.11.015.

[49] Y.Q. Li, B.H. Zhao, X.T. Chen, Y.Q. Zhang, H.S. Yang, Co-existence effect of copper oxide nanoparticles and ciprofloxacin on simultaneous nitrification, endogenous denitrification, and phosphorus removal by aerobic granular sludge, Chemosphere 312 (2023), https://doi.org/10.1016/j.chemosphere.2022.137254.

[50] X.Y. Zheng, D. Lu, W. Chen, Y.J. Gao, G. Zhou, Y. Zhang, X. Zhou, M.Q. Jin, Response of aerobic granular sludge to the long-term presence of CuO NPs in A/O/A SBRs: nitrogen and phosphorus removal, enzymatic activity, and the microbial community, Environ. Sci. Technol. 51 (2017) 10503–10510, https://doi.org/10.1021/acs.est.7b02768.

[51] Y. Jiang, Y. Shang, W. Zhang, X. Zhang, J. Li, S. Shao, Assessing the effect of SiO2 and TiO2 nanoparticles on granule stability and microbial community shift in aerobic granular sludge process, Chemosphere 307 (2022) 135677, https://doi.org/10.1016/j.chemosphere.2022.135677.

[52] B. Li, W. Huang, C. Zhang, S. Feng, Z. Zhang, Z. Lei, N. Sugiura, Effect of TiO2 nanoparticles on aerobic granulation of algal-bacterial symbiosis system and nutrients removal from synthetic wastewater, Bioresour. Technol. 187 (2015) 214–220, https://doi.org/10.1016/j.biortech.2015.03.118.

[53] M. Xiao, J. Xin, J. Fan, B. Ji, Response mechanisms of microalgal-bacterial granular sludge to zinc oxide nanoparticles, Bioresour. Technol. 361 (2022) 127713, https://doi.org/10.1016/j.biortech.2022.127713.

[54] A.G. Dymerska, B. Środa, B. Zielińska, E. Mijowska, Ni-MOF-based electrodes: a promising strategy for efficient overall water splitting, Electrochim. Acta 462 (2023), https://doi.org/10.1016/j.electacta.2023.142725.

[55] Y. Zeng, L. Wang, Z. Wang, J. Xiao, H. Wang, Facile synthesis of self-assembled porous NiO nanostructures and their application to supercapacitor electrodes, Mater. Today Commun. 5 (2015) 70–74, https://doi.org/10.1016/j.mtcomm.2015.11.001.

[56] A. Kedves, L. Sánta, M. Balázs, P. Kesserű, I. Kiss, A. Rónavári, Z. Kónya, Chronic responses of aerobic granules to the presence of graphene oxide in sequencing batch reactors, J. Hazard Mater. 389 (2020), https://doi.org/10.1016/j.jhazmat.2019.121905.

[57] N. Zhou, Z. Zhao, H. Wang, X. Chen, M. Wang, S. He, W. Liu, M. Zheng, The effects of graphene oxide on nitrification and N2O emission: dose and exposure time dependent, Environ. Pollut. 252 (2019) 960–966, https://doi.org/10.1016/j.envpol.2019.06.009.

[58] J. Zeng, J.M. Gao, Y.P. Chen, P. Yan, Y. Dong, Y. Shen, J.S. Guo, N. Zeng, P. Zhang, Composition and aggregation of extracellular polymeric substances (EPS) in hyperhaline and municipal wastewater treatment plants, Sci. Rep. 6 (2016) 1–9, https://doi.org/10.1038/srep26721.

[59] M. Bonomo, Synthesis and characterization of NiO nanostructures: a review, J. Nanoparticle Res. 20 (2018) 222, https://doi.org/10.1007/s11051-018-4327-y.

[60] K. Motevalli, Z. Zarghami, M. Panahi-Kalamuei, Simple, novel and low-temperature synthesis of rod-like NiO nanostructure via thermal decomposition route using a new starting reagent and its photocatalytic activity assessment, J. Mater. Sci. Mater. Electron. 27 (2016) 4794–4799, https://doi.org/10.1007/s10854-016-4360-5.

[61] S.P. Patil, L.D. Jadhav, D.P. Dubal, V.R. Puri, Characterization of NiO-Al2O3 composite and its conductivity in biogas for solid oxide fuel cell, Mater. Sci. Pol. 34 (2016) 266–274, https://doi.org/10.1515/msp-2016-0045.

[62] K.C. Devarayapalli, S.V.P. Vattikuti, S. Tvm, K.S. Yoo, P.C. Nagajyothi, J. Shim, Facile synthesis of Ni-MOF using microwave irradiation method and application in the photocatalytic degradation, Mater. Res. Express 6 (2019), https://doi.org/10.1088/2053-1591/ab5261.

[63] A.H.A. Rahim, S.N.F. Yusuf, S.R. Majid, Z. Osman, One-step co-precipitated β-Ni(OH)2 at different ratios of Ni/2-methylimidazole and its energy storage behaviour, J. Appl. Electrochem. 52 (2022) 159–172, https://doi.org/10.1007/s10800-021-01627-0.

[64] D.S. Hall, D.J. Lockwood, C. Bock, B.R. MacDougall, Nickel hydroxides and related materials: a review of their structures, synthesis and properties, Proc. R. Soc. A Math, Phys. Eng. Sci. 471 (2015), https://doi.org/10.1098/rspa.2014.0792.

[65] T. Ueda, T. Yamatani, M. Okumura, Dynamic gate opening of ZIF-8 for bulky molecule adsorption as studied by vapor adsorption measurements and computational approach, J. Phys. Chem. C 123 (2019) 27542–27553, https://doi.org/10.1021/acs.jpcc.9b07239.

[66] Y. Ren, L. Li, N. Liu, K. Zhang, C. Li, Z. Chen, B. Zhang, Quasi-vertical GaN heterojunction diodes with p-NiO anodes deposited by sputtering and post-annealing, Vacuum 182 (2020) 109784, https://doi.org/10.1016/j.vacuum.2020.109784.

[67] H. Wang, C. Zhu, M. Wu, F. Zheng, Y. Gao, H. Niu, Synthesis of a novel double-ligand nickel conductive metal–organic framework material and its electrochemical characterization for supercapacitors, J. Mater. Sci. 56 (2021) 2517–2527, https://doi.org/10.1007/s10853-020-05378-9.

[68] W. Li, X. Yang, Q. Hou, X. Lu, J. Kong, J. Su, Modification of MgH_2 hydrogen storage performance by nickel-based composite catalyst Ni/NiO, Heliyon 10 (2024) e30688, https://doi.org/10.1016/j.heliyon.2024.e30688.

[69] H. Shooshtari Gugtapeh, M. Rezaei, One-step electrodeposition of a mesoporous Ni/Co-Imidazole-Based bimetal-organic framework on pyramid-like NiSb with abundant coupling interfaces as an ultra-stable heterostructural electrocatalyst for water splitting, ACS Appl. Mater. Interfaces 15 (2023) 34682–34697, https://doi.org/10.1021/acsami.3c03021.

[70] S. Shin, M.W. Shin, Nickel metal–organic framework (Ni-MOF) derived NiO/C@CNF composite for the application of high performance self-standing supercapacitor electrode, Appl. Surf. Sci. 540 (2021) 148295, https://doi.org/10.1016/j.apsusc.2020.148295.

[71] H.Y. Mohammed, M.A. Farea, M.N. Murshed, V.N. Narwade, K.B. Deore, M.D. Shirsat, A nickel -metal–organic framework for an efficient and stable electrode for the oxygen evolution reaction and energy storage, Mater, Today Proc. 92 (2023) 626–631, https://doi.org/10.1016/j.matpr.2023.04.127.

[72] G. George, S. Anandhan, Synthesis and characterisation of nickel oxide nanofibre webs with alcohol sensing characteristics, RSC Adv. 4 (2014) 62009–62020, https://doi.org/10.1039/c4ra11083h.

[73] D. Saravanak Kumar, S. Sabapathi Pandiarajan, D. Saravanakkumar, R. Karthika, S. Ganasaravanan, S. Sivaranjani, B. Ravikumar, A. Ayeshamariam, Synthesis of NiO doped ZnO/MWCNT nanocomposite and its charecterization for photocatalytic & antimicrobial applications, artic, IOSR J. Appl. Phys. 10 (2018) 73–83, https://doi.org/10.9790/4861-1003027383.
[74] A.D. Sontakke, A. Bhattacharjee, R. Fopase, L.M. Pandey, M.K. Purkait, One-pot, sustainable and room temperature synthesis of graphene oxide-impregnated iron-based metal-organic framework (GO/MIL-100(Fe)) nanocarriers for anticancer drug delivery systems, J. Mater. Sci. 57 (2022) 19019–19049, https://doi.org/10.1007/s10853-022-07773-w.
[75] Z. Huang, L. Zhang, P. Cao, N. Wang, M. Lin, Electrochemical sensing of dopamine using a Ni-based metal-organic framework modified electrode, Ionics 27 (2021) 1339–1345, https://doi.org/10.1007/s11581-020-03857-2.
[76] Y. Wang, S. Liu, Q. Guo, Y. Zhang, Ni@C@CNT catalyst derived from CNT doped Ni-MOF for furfural hydrogenation to tetrahydrofurfuryl alcohol, Asia-Pacific, J. Chem. Eng. 17 (2022) 1–10, https://doi.org/10.1002/apj.2739.
[77] E.P. Asiwal, D.S. Shelar, C.S. Gujja, S.T. Manjare, S.D. Pawar, A Ni-MOF based luminescent sensor for selective and rapid sensing of Fe(ii) and Fe(iii) ions, New J. Chem. 46 (2022) 12679–12685, https://doi.org/10.1039/d2nj02263j.
[78] N. Hu, J. Liao, X. Liu, J. Wei, L. Wang, M. Li, N. Zong, R. Xu, L. Yang, J. Wang, CNTs support 2D NiMOF nanosheets for asymmetric supercapacitors with high energy density, Dalton Trans. 51 (2022) 16344–16353, https://doi.org/10.1039/D2DT02055F.
[79] G. Manibalan, G. Murugadoss, P. Kuppusami, N. Kandhasamy, M. Rajesh Kumar, Synthesis of heterogeneous NiO nanoparticles for high-performance electrochemical supercapacitor application, J. Mater. Sci. Mater. Electron. 32 (2021) 5945–5954, https://doi.org/10.1007/s10854-021-05315-9.
[80] Z.-Z. Zhang, J.-J. Xu, Z.-J. Shi, Y.-F. Cheng, Z.-Q. Ji, R. Deng, R.-C. Jin, Combined impacts of nanoparticles on anammox granules and the roles of EDTA and S2− in attenuation, J. Hazard Mater. 334 (2017) 49–58, https://doi.org/10.1016/j.jhazmat.2017.04.002.
[81] Y. Xue, H. Ma, Y. Hu, Z. Kong, Y.-Y. Li, Microstructure and granulation cycle mechanisms of anammox-HAP coupled granule in the anammox EGSB reactor, Water Res. 210 (2022) 117968, https://doi.org/10.1016/j.watres.2021.117968.
[82] B. Ma, Z. Li, S. Wang, Z. Liu, S. Li, Z. She, N. Yu, C. Zhao, C. Jin, Y. Zhao, L. Guo, M. Gao, Insights into the effect of nickel (Ni(II))on the performance, microbial enzymatic activity and extracellular polymeric substances of activated sludge, Environ. Pollut. 251 (2019) 81–89, https://doi.org/10.1016/j.envpol.2019.04.094.
[83] L. Liu, Z. Zeng, M. Bee, V. Gibson, L. Wei, X. Huang, C. Liu, Characteristics and performance of aerobic algae-bacteria granular consortia in a photo-sequencing batch reactor, J. Hazard Mater. 349 (2018) 135–142, https://doi.org/10.1016/j.jhazmat.2018.01.059.
[84] W. Xiong, S. Wang, Y. Jin, Z. Wu, D. Liu, H. Su, Insights into nitrogen and phosphorus metabolic mechanisms of algal-bacterial aerobic granular sludge via metagenomics: performance, microbial community and functional genes, Bioresour. Technol. 369 (2023) 128442, https://doi.org/10.1016/j.biortech.2022.128442.
[85] W. Huang, B. Li, C. Zhang, Z. Zhang, Z. Lei, B. Lu, B. Zhou, Effect of algae growth on aerobic granulation and nutrients removal from synthetic wastewater by using sequencing batch reactors, Bioresour. Technol. 179 (2015) 187–192, https://doi.org/10.1016/j.biortech.2014.12.024.
[86] Z. Wang, M. Gao, Z. She, S. Wang, C. Jin, Y. Zhao, S. Yang, L. Guo, Effects of salinity on performance, extracellular polymeric substances and microbial community of an aerobic granular sequencing batch reactor, Sep. Purif. Technol. 144 (2015) 223–231, https://doi.org/10.1016/j.seppur.2015.02.042.
[87] S. Wang, M. Gao, Z. She, D. Zheng, C. Jin, L. Guo, Y. Zhao, Z. Li, X. Wang, Long-term effects of ZnO nanoparticles on nitrogen and phosphorus removal, microbial activity and microbial community of a sequencing batch reactor, Bioresour. Technol. 216 (2016) 428–436, https://doi.org/10.1016/j.biortech.2016.05.099.
[88] Q. Xu, S. Li, Y. Wan, S. Wang, B. Ma, Z. She, L. Guo, M. Gao, Y. Zhao, C. Jin, J. Dong, Z. Li, Impacts of silver nanoparticles on performance and microbial community and enzymatic activity of a sequencing batch reactor, J. Environ. Manag. 204 (2017) 667–673, https://doi.org/10.1016/j.jenvman.2017.09.050.
[89] S. Wang, M. Gao, Z. Li, Z. She, J. Wu, D. Zheng, L. Guo, Y. Zhao, F. Gao, X. Wang, Performance evaluation, microbial enzymatic activity and microbial community of a sequencing batch reactor under long-term exposure to cerium dioxide nanoparticles, Bioresour. Technol. 220 (2016) 262–270, https://doi.org/10.1016/j.biortech.2016.08.086.
[90] S. Rezania, H. Kamyab, P.F. Rupani, J. Park, N. Nawrot, E. Wojciechowska, K.K. Yadav, M. Lotfi Ghahroud, A.A. Mohammadi, S.T. Thirugnana, S. Chelliapan, M. M.S. Cabral-Pinto, Recent advances on the removal of phosphorus in aquatic plant-based systems, Environ. Technol. Innov. 24 (2021) 101933, https://doi.org/10.1016/j.eti.2021.101933.
[91] X. Xiao, W. Li, M. Jin, L. Zhang, L. Qin, W. Geng, Responses and tolerance mechanisms of microalgae to heavy metal stress: a review, Mar. Environ. Res. 183 (2023) 105805, https://doi.org/10.1016/j.marenvres.2022.105805.
[92] X. Zheng, Y. Zhang, W. Chen, W. Wang, H. Xu, X. Shao, M. Yang, Z. Xu, L. Zhu, Effect of increased influent COD on relieving the toxicity of CeO2 NPs on aerobic granular sludge, Int. J. Environ. Res. Publ. Health 16 (2019), https://doi.org/10.3390/ijerph16193609.
[93] W. Liu, J. Zhang, Y. Jin, X. Zhao, Z. Cai, Adsorption of Pb(II), Cd(II) and Zn(II) by extracellular polymeric substances extracted from aerobic granular sludge: efficiency of protein, J. Environ. Chem. Eng. 3 (2015) 1223–1232, https://doi.org/10.1016/j.jece.2015.04.009.
[94] Q. He, S. Gao, S. Zhang, W. Zhang, H. Wang, Chronic responses of aerobic granules to zinc oxide nanoparticles in a sequencing batch reactor performing simultaneous nitrification, denitrification and phosphorus removal, Bioresour. Technol. 238 (2017) 95–101, https://doi.org/10.1016/j.biortech.2017.04.010.